Association and Redox Properties of the Putidaredoxin Reductase−Nicotinamide Adenine Dinucleotide Complex

Vytas Reipa,[‡] Marcia J. Holden,[‡] and Vincent L. Vilker*[,‡,§,⊥]

National Institute of Standards and Technology, 100 Bureau Drive, Gaithersburg, Maryland, Center for Advanced Research in Biotechnology, 9600 Gudelsky Drive, Rockville, Maryland, and U.S. Food and Drug Administration, White Oak Building 22, Room 2130, 10903 New Hampshire Avenue, Silver Spring, Maryland

Received June 19, 2007; Revised Manuscript Received September 4, 2007

ABSTRACT: Putidaredoxin reductase (PdR) is the flavin protein that carries out the first electron transfer involved in the cytochrome P450cam catalytic cycle. In PdR, the flavin adenine dinucleotide (FAD/$FADH_2$) redox center acts as a transformer by accepting two electrons from soluble nicotinamide adenine dinucleotide (NAD^+/NADH) and donating them in two separate, one-electron-transfer steps to the iron−sulfur protein putidaredoxin (Pdx). PdR, like the two more intensively studied monoflavin reductases, adrenodoxin reductase (AdR) and ferredoxin−$NADP^+$ reductase (FNR), has no other active redox moieties (e.g., sulfhydryl groups) and can exist in three different oxidation states: (i) oxidized quinone, (ii) one-electron reduced semiquinone (stable neutral species (blue) or unstable radical anion (red)), and (iii) two-electron fully reduced hydroquinone. Here, we present reduction potential measurements for PdR in support of a thermodynamic model for the modulation of equilibria among the redox components in this initial electron-transfer step of the P450 cycle. A spectroelectrochemical technique was used to measure the midpoint oxidation−reduction potential of PdR that had been carefully purified of all residual NAD^+, $E^{0\prime} = -369 \pm 10$ mV at pH 7.6, which is more negative than previously reported and more negative than the pyridine nucleotide NADH/NAD^+ (−330 mV). After addition of NAD^+, the formation of the oxidized reductase-oxidized pyridine nucleotide complex was followed by the two-electron-transfer redox reaction, PdR^{ox}:$NAD^+ + 2e^- \rightarrow PdR^{rd}$:$NAD^+$, when the electrode potential was lowered. The midpoint potential was a hyperbolic function of increasing NAD^+ concentration, such that at concentrations of pyridine nucleotide typically found in an intracellular environment, the midpoint potential would be $E^{0\prime} = -230 \pm 10$ mV, thereby providing the thermodynamically favorable redox equilibria that enables electron transfer from NADH. This thermodynamic control of electron transfer is a shared mechanistic feature with the adrenodoxin P450 and photosynthetic electron-transfer systems but is different from the kinetic control mechanisms in the microsomal P450 systems where multiple reaction pathways draw on reducing power held by NADPH−cytochrome P450 reductase. The redox measurements were combined with protein fluorescence quenching of NAD^+ binding to oxidized PdR to establish that the PdR^{ox}:NAD^+ complex ($K_D = 230$ μM) is about 5 orders of magnitude weaker than PdR^{rd}:NAD^+ binding. These results are integrated with known structural and kinetic information for PdR, as well as for AdR and FNR, in support of a compulsory ordered pathway to describe the electron-transfer processes catalyzed by all three reductases.

Putidaredoxin reductase PdR[1] is the flavin protein (46 kDa; E.C. 1.18.1.3) that carries out the first electron transfer involved in the cytochrome P450cam catalytic cycle. The crystal structure has recently been published (*1*). PdR function has been the subject of numerous investigations (*2*−*4*), especially for making comparisons with adrenodoxin reductase (AdR), its functional analog in the catalytic cycle of the adrenal steroid-hydroxylating cytochrome P450scc (*5*−*7*). In PdR, the flavin adenine dinucleotide (FAD/$FADH_2$) redox center is reduced by two-electron transfer from nicotinamide adenine dinucleotide (NAD^+/NADH). PdR channels these reducing equivalents via the iron−sulfur protein putidaredoxin (Pdx) to the terminal cytochrome P450 enzyme via two separate, one-electron transfers. These PdR-to-Pdx electron-transfer steps of the P450 cycle are not nearly so systematically characterized as are the terminal steps of the catalytic cycle where the heme P450 enzyme, along with hydrocarbon and oxygen substrates and Pdx, converge for completion of the hydroxylation reaction. Sligar and Gunsalus (*8*, *9*), Peterson and colleagues (*10*, *11*), and Kuznetsov et al. (*12*) furnish the measurements and concepts leading to our understanding of the driving forces and coupling

* To whom correspondence should be addressed. Tel.: +1 301 796 0200. Fax: +1 301 796 9859. E-mail: Vincent.Vilker@fda.hhs.gov.
‡ National Institute of Standards and Technology.
§ Center for Advanced Research in Biotechnology.
⊥ U.S. Food and Drug Administration.

[1] Abbreviations: $E^{0\prime}$, midpoint oxidation reduction potential; PdR, putidaredoxin reductase; PdR^{ox}, putidaredoxin reductase in oxidized state; PdR^{rd}, putidaredoxin in reduced state; PdR^{ox}:NAD^+, putidaredoxin reductase in oxidized state with bound oxidized pyridine nucleotide; AdR, adrenodoxin reductase; FNR, ferredoxin−$NADP^+$ reductase; Pdx, putidaredoxin; Adx, adrenodoxin; Fd, ferredoxin.

10.1021/bi7012118 CCC: $37.00
Published on Web 10/17/2007

equilibria in these final reactions of the catalytic cycle. In this article, we present reduction potential measurements for PdR in support of a thermodynamic model for the modulation of the equilibria among the redox components in the initial electron-transfer step.

Flavoproteins like PdR and AdR, with no other active redox moieties (e.g., sulfhydryl groups), can exist in three different oxidation states: (i) oxidized quinone, (ii) one-electron reduced semiquinone (stable neutral species (blue) or unstable radical anion (red)), and (iii) two-electron fully reduced hydroquinone. These states are in dynamic equilibria with one another, and the distribution of states is affected by the character of the apoprotein and often by ligands that bind to the protein (*13*). This distribution of redox states plays a critical role in determining the direction and ease of electron transfer with the many potential redox partners with which the flavoprotein interacts in a typical intracellular environment. Indeed, stabilization of the semiquinone state gives some flavoproteins the ability to split electrons between obligatory one- and two-electron carriers. This appears to be the case especially with reductases that are known to furnish reducing power to microsomal P450s (*14*−*16*). Semiquinone stability (instability) is critical to the one- versus two-electron delivery by ferredoxin−$NADP^+$ reductase, the terminal monoflavin protein in the photosynthetic chain (*17*−*21*). In AdR, stabilization of the semiquinone state has been identified with the protonation of the FAD isoalloxazine N5 atom by a water molecule fixed by hydrogen bonds to residues surrounding the redox center (*22*). However, in addition to these structural features, the electron transfer from NADPH to AdR is also strongly influenced by binding of $NADP^+$ ligand (*5*, *6*). The structure of PdR has not been found to support stabilization of the semiquinone radical (*1*), but binding of NAD^+ is an important influence on PdR electron-transfer function through mediation of its redox potential (*23*, *24*).

Previous measurements of oxidation/reduction potential for PdR two-electron transfer give −285 (*25*) and −320 mV (*26*) by dye photoreduction methods or −270 to −317 mV by titration with NADPH or NADH (*23*, *27*). The influence of the tight binding of the oxidized pyridine nucleotide to PdR on oxidation/reduction potential has not been studied systematically, in part because this binding is sufficiently strong so that pyridine nucleotide is copurified with PdR whether the protein is purified from the natural source (camphor-induced expression in *Pseudomonas putida*), or as recombinant protein from *E. coli* cultures for determination of the PdR structure by X-ray diffraction (*1*). At the most positive values of this reported range, and using the formal potential for the NADH/NAD^+ couple to be −330 mV (*28*), the rationale for thermodynamic mediation of electron transfer from the pyridine nucleotide into the P450cam cycle is on reasonable standing; however, the more negative potential measurements raise issues with this concept and open up the need to consider other driving forces to supply reducing power, as in the case of the microsomal P450 catalytic cycles (*29*).

The goals of this work were (i) to explore and quantify the binding of the oxidized pyridine nucleotide NAD^+ with oxidized and reduced PdR, (ii) to measure the midpoint oxidation−reduction potential of PdR as a function of NAD^+ concentration, (iii) to develop a thermodynamic model for the modulation of PdR redox equilibrium, and (iv) to contribute understanding of the comparative mechanisms for electron transfer to the monoflavin reductases of the bacterial, mitochondrial, and microsomal P450 cycles, and those that serve as the terminal enzymes of the photosynthetic electron transport chain.

EXPERIMENTAL PROCEDURES

Protein Preparation. Putidaredoxin reductase was obtained by heterologous expression in *E. coli* clones using growth, purification, and catalytic reconstitution procedures described in ref *2*. Protein released from harvested cells (4−5 mg PdR/g cell paste) was purified in three chromatographic steps using media from Pharmacia Biotech:[2] ion-exchange using DEAE Sepharose (20−40% purity), hydrophobic interaction (HIC) using Phenyl Sepharose 6 FF (60−80% purity), and size exclusion using Sephacryl S-200HR (>98% purity). In the single redox titration experiment where we wanted to ensure that there was no residual bound NAD^+, NAD was removed from an aliquot of the PdR preparations as per the methods described in ref *30*. Briefly, the protein was unfolded using 8 M guanidine HCl, followed by separation of the protein from small molecules using size-selective membranes and protein refolding in the presence of FAD to reconstitute the active protein.[3] Absorbance of this preparation (NAD-free PdR) was measured from 350 to 550 nm prior to unfolding and after the final refolding wash. Spectra were superimposable with the characteristic peaks at 378, 454, and 480 nm. These spectra were distinctly different relative to similar spectra for free, unbound FAD. The quantitation of the folded protein was based on absorbance at 454 nm ($\epsilon = 10\ mM^{-1}\ cm^{-1}$) (*25*).

Spectroelectrochemical Redox Titration and Equilibrium Binding Measurements. Spectroelectrochemical experiments were conducted using a thin-layer quartz cell (Figure 1) that provides exhaustive electrolysis in a sandwiched solution layer (*31*−*33*). The absorbance of protein solution in the 0.1 mm gap between two electrodes coated with nanocrystalline antimony-doped tin oxide (*31*, *32*) was measured in the direction parallel to working electrode surfaces, providing a

[2] Certain commercial equipment, instruments, and materials are identified in this paper to specify adequately the experimental procedure. In no case does such identification imply recommendation or endorsement by the National Institute of Standards and Technology or the FDA, nor does it imply that the material or equipment is necessarily the best available for the purpose.

[3] PdR (100−200 nmol, >98% pure) was added to 50−100 mL of denaturation buffer (50 mM Tris−HCl, 200 mM KCl, 8 M guanidine−HCl, 2 mM DTT, pH 7.4) and stirred slowly on ice for an hour. The solution was reduced in volume to <10 mL using an Amicon stirred cell (200 mL volume) equipped with a YM10 membrane (10 K MW cutoff). The protein solution was transferred to 4 mL centrifugal concentrators with YM10 membranes and reduced in volume further (~0.5 mL). Additional denaturation buffer (4 mL) was added to the concentrated protein solution, and the centrifugation was repeated to wash the protein free of small molecules. This step was repeated four or more additional times. The final volume of protein retrieved from the concentrator was about 1 mL. PdR was refolded in the presence of FAD by very slow addition to a stirred solution of renaturation buffer (50 mM Tris−HCl, 200 mM KCl, 200 mM guanidine HCl, 1 mM DTT, 25 μM FAD, pH 7.4). The solution was stirred on ice for 1 h and then reduced in volume using the Amicon cell and then centrifugal concentrators as before. Finally, the protein was washed in a centrifugal concentrator with a buffer of 50 mM Tris−HCl buffer, 200 mM KCl, pH 7.4 until all free FAD was removed from the protein solution.

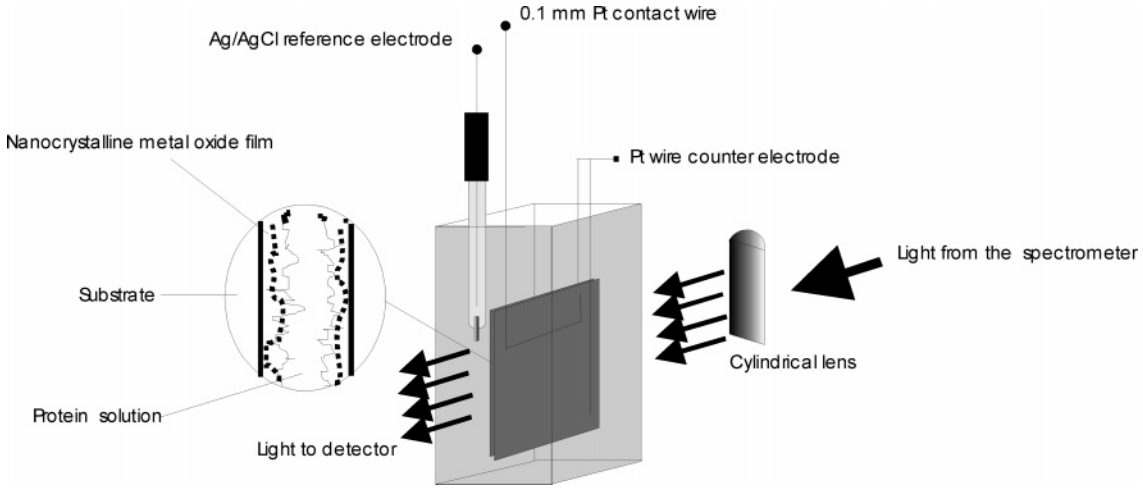

FIGURE 1: Schematic of the thin-layer spectroelectrochemical cell used for protein absorbance measurements. A nanocrystalline metal oxide film was sol−gel coated on glass substrates as shown in the inset. The absorbance of protein solution in the 0.1 mm gap between two electrodes coated with nanocrystalline antimony-doped tin oxide is measured in the direction parallel to the working electrode surfaces (5 mm optical path length). The working electrodes are pressed against a 0.1 mm Pt wire that serves as the 0.1 mm spacer and provides an electrical contact. The gap between the electrodes fills due to capillary action, thus minimizing total solution volume. The airtight quartz cell also contains a Pt wire counter electrode, Ag/AgCl reference (Microelectrodes, Inc., Bedford, NH), and provides for solution and Ar gas delivery.

5 mm optical path length. Before titration, solutions were poised at the initial potential for at least 2 h while purging with oxygen-free, water-saturated Ar gas. A gas blanket was maintained in the cell headspace during the anaerobic potential scans. The reference electrode was placed outside the gap, and the cell was calibrated against phenosafranine ($E^{0\prime} = -257$ mV vs NHE) as an internal standard. Solutions for the spectroelectrochemical titration contained 0.2 M KCl, 0.02 M $MgCl_2$, 0.05 M Tris−HCl, pH 7.6, and also a mediator soup (1 μM each: phenazine methosulfate $E^{0\prime} = +140$ mV; indigo carmine, $E^{0\prime} = -125$ mV; phenosafranine, $E^{0\prime} = -257$ mV; benzyl viologen, $E^{0\prime} = -330$ mV; methyl viologen, $E^{0\prime} = -450$ mV). Addition of small concentrations of multivalent cation Mg^{2+} and the mediator soup facilitate electron transfer between redox proteins and metal oxide electrodes (*31*, *33*). All experiments were conducted at 20 °C using the thermoelectric cell holder (Quantum Northwest, Spokane, WA). Typically, absorbance was recorded every 3 mV at several wavelengths during the 0.05 mV/s potential ramp. All potentials are given with respect to the standard hydrogen electrode (SHE).

Equilibrium binding of oxidized pyridine nucleotide NAD^+ to oxidized putidaredoxin reductase was determined using absorption difference spectrophotometry (*34*, *35*) and an NAD^+-dependent fluorescence quenching method (*35*, *36*). Preliminary measurements by both methods indicated relatively weak binding ($K_D \sim 200-350$ μM), although the fluorescence quenching method gave more reproducible results for repeated experimental trials with different preparations of protein and pyridine nucleotide. In the fluorescence quenching method, the attenuation of the fluorescence of the aromatic residues in the range of 310−340 nm of 20 μM PdR solutions excited at 290 nm was recorded using a LM800 spectrofluorimeter (SLM Inc.). Small aliquots of 20 mM NAD^+ solution were mixed to a 7.5 mM final concentration, and fluorescence emission reading at 338 nm was plotted as a function of NAD^+ concentration (Figure 7). The fluorescence intensity of *N*-acetyltryptophaneamide as a function of NAD^+ concentration was used to correct for the absorptive screening by NAD^+ at the excitation wavelength. Data were fit to a single-site model of NAD^+ binding (*4*, *23*) with the dissociation constant determined by a Scatchard plot.

RESULTS

PdR Redox Potential without and with NAD. The absorbance spectra of oxidized, NAD-free PdR, recorded during the potential sweep from −100 (top curves of Figure 2, parts A and B) to −500 mV (bottom curves) in the thin-layer cell, contains maxima at 380, 454, and a shoulder at 480 nm, typical for the FAD domain. When the electrode potential was scanned in the direction of more negative values, there was a gradual reduction of the flavin moiety, as indicated by decreases in the main absorbance peaks. Spectral changes were fully reversible when the potential was returned to the initial value (−100 mV). Absorbance changes at wavelengths >520 nm were insignificant throughout the anaerobic reduction of the 9 μM PdR solution, suggesting the absence of significant quantities of semiquinone species (*14*, *37*).

Figure 2B shows the long-wavelength band (>600 nm) that appears during the reduction of PdR in the presence of 5× excess NAD^+. The intensity of this band grows in parallel with the decrease in FAD center absorbance. Such absorbance features are indicative of charge-transfer complex formation between reduced PdR and oxidized pyridine nucleotide (*37*). The absorbance increases in Figure 2B at wavelengths <350 nm reflect NADH formation that follows FAD reduction.

The evolution of the NAD-free PdR redox state was followed at 454 nm during the 0.05 mV/s linear scan (Figure 3). This spectroelectrochemical titration gives the slope 35 ± 5 mV/decade corresponding to two-electron transfer, and the midpoint reduction potential of −369 ± 10 mV, a value that is significantly more negative than the midpoint potential of its biological electron source NAD^+/NADH, $E^{0\prime} = -330$ mV at pH 7.6 (*28*).

Upon addition of 45 μM NAD^+, the spectroelectrochemical measurements shown in Figure 4 indicate that the PdR

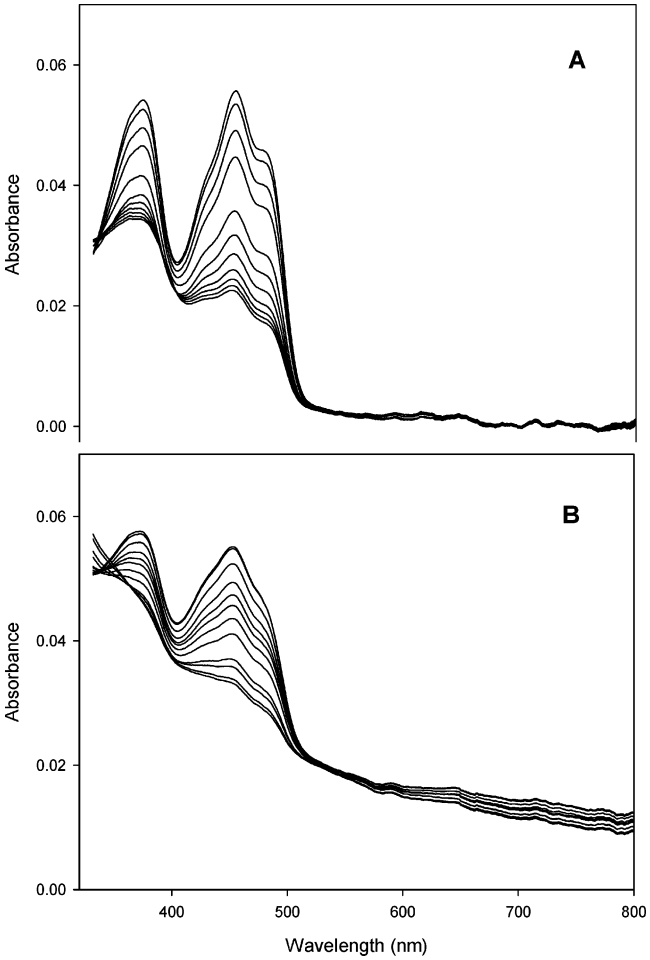

FIGURE 2: Reduction/oxidation absorbance spectra of NAD-free PdR without added NAD^+ (A) and with 45 μM NAD^+ (B). Spectra were acquired in a thin-layer spectroelectrochemical cell at 20 °C. PdR (9 μM) was titrated in deaerated 50 mM Tris buffer (pH 7.6) also containing 200 mM KCl and 20 mM $MgCl_2$. Spectra were recorded during potential sweeps from −100 (top spectra) to −500 mV (bottom spectra) at 0.05 mV/s.

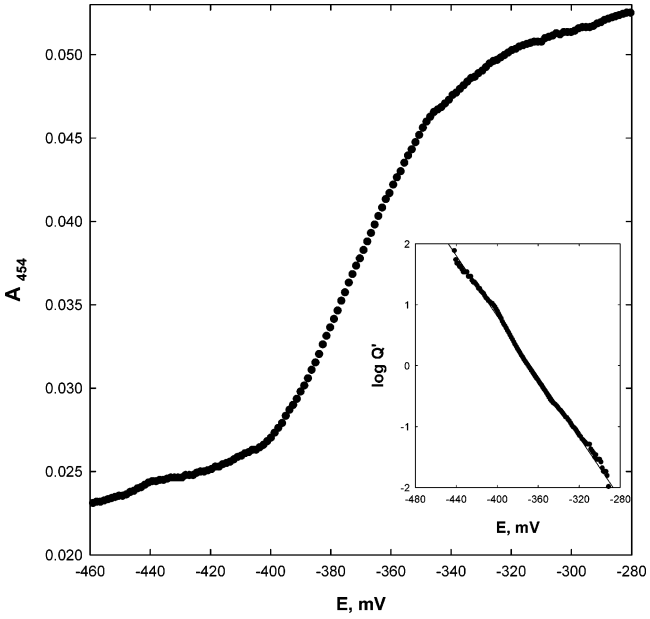

FIGURE 3: Absorbance change at 454 nm as function of electrode potential recorded in same solution as Figure 2 with 9 μM NAD-free PdR. The redox wave centered on about −370 mV is used to find the reduction/oxidation midpoint potential of the reaction $PdR^{ox} + 2e^- \rightarrow PdR^{rd}$ from the Nernst equation $E = E^{0\prime} - (RT/nF) \ln Q'$ (where E is applied potential; the reaction quotient $Q' = [PdR^{rd}]/[PdR^{ox}] = (1 - x)/x$, with $x = (A - A^{rd})/(A^{ox} - A^{rd})$, during the roundtrip potential scans between −50 and −500 mV at 0.05 mV/s; A is absorbance at 454 nm with A^{rd} for fully reduced PdR^{rd} and A^{ox} for fully oxidized PdR^{ox}). The inset shows log Q' to be linear for 4 orders of magnitude of E giving the slope 35 ± 5 mV/decade for this two-electron process and midpoint reduction potential of −369 ± 10 mV.

redox wave shifts to −268 ± 10 mV, more than 100 mV more positive than the NAD-free PdR midpoint potential. The Nernst slope (Figure 4 inset) in the presence of NAD^+ indicates two-electron transfer, the same as the neat PdR titration. Absorbance bleaching at 454 nm starts at $E < -190$ mV together with the formation of the PdR:NAD^+ charge-transfer complex as monitored by the absorbance rise at 750 nm. The rise in 340 nm absorbance for $E < -300$ mV, just as PdR reduction is nearly completed, indicates NADH formation. Since this 340 nm absorbance rise is proportional to the amount of total added NAD^+ (data not shown), this rise is consistent with reduction of free, unassociated NAD^+.

Given that NAD^+ induces a positive PdR redox potential shift, we conducted the series of PdR spectroelectrochemical titrations with varying amounts of NAD^+ shown in Figure 5A. All experiments were conducted in 9 μM PdR solutions with NAD^+/PdR molar ratio ranging from 0 to 33. The values of $E^{0\prime}$ for PdR, calculated from Nernst plots of the titration curves, show that $E^{0\prime}$ asymptotes to −230 mV at high concentrations of NAD^+ (Figure 5B). This indicates that in the presence of oxidized pyridine nucleotide, $E^{0\prime}$ is shifted sufficiently positive to create thermodynamically favorable conditions for the electron transfer from NADH to PdR. Addition of similar amounts of $NADP^+$ did not produce a measurable effect on PdR titration curves (data not shown).

Upon addition of putidaredoxin (Pdx) to a concentration that is in 2-fold molar excess of PdR, the spectroelectrochemical measurements shown in Figure 6 indicate that the midpoint potential of PdR:NAD^+ is unaffected by this natural redox partner of PdR. The redox wave centered at −289 mV is comparable to the PdR titration redox wave without Pdx (curve c in Figure 5A). This redox wave at A_{454} in Figure 6 has a slightly more rapid absorbance decrease than curve c of Figure 5A for $E \geq \approx -250$ mV due to considerable overlap with a Pdx redox wave ($E^{0\prime} \approx -240$ mV). The rise in 750 nm absorbance (dotted line) reflects formation of the PdR:NAD^+ charge complex.

Binding of NAD^+ and PdR^{ox}. Equilibrium binding of NAD^+ to oxidized putidaredoxin reductase was determined by measuring fluorescence quenching of PdR due to NAD^+ association. Figure 7 shows the decline in fluorescence for increasing total NAD^+, relative to an initial value for free, unbound 20 μM PdR^{ox}. These data were fit to a single-site model of NAD^+ binding (*4*, *23*):

$$PdR^{ox} + NAD^+ \underset{K_3=1/K_{D3}}{\rightleftharpoons} PdR^{ox}{:}NAD^+$$

where K_{D3} is the dissociation constant determined by a Scatchard plot: $K_{D3} = 230 \pm 30$ μM.

DISCUSSION

PdR Midpoint Reduction Potential as a Function of NAD^+. First attempts to make precision measurements of the

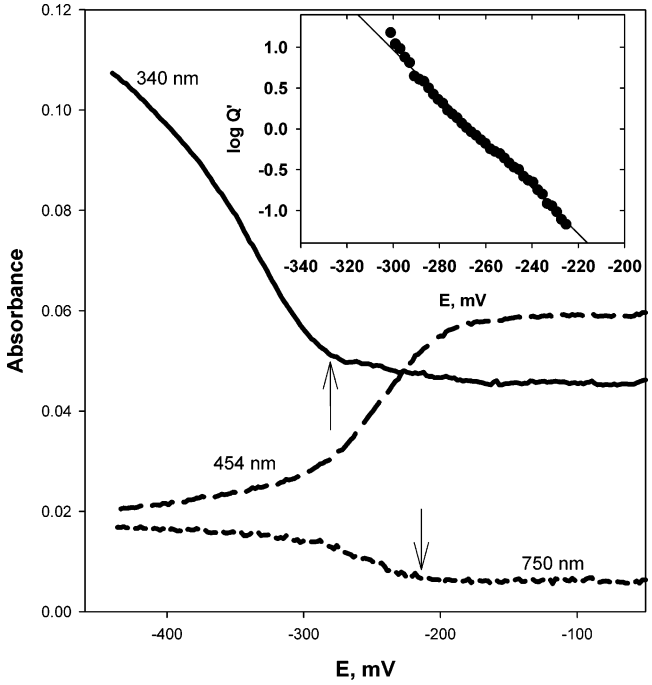

FIGURE 4: Absorbance changes as function of electrode potential for 9 μM PdR and 45 μM NAD^+. Reduction of PdR^{ox}, evolution of PdR:NAD^+ complex, and reduction of NAD^+ are followed simultaneously at 454, 750, and 340 nm, respectively. The lower arrow indicates the beginning of formation of the reduced charge-transfer complex as the potential is made more negative from −100 mV, and the upper arrow indicates the onset of NAD^+ reduction (see text). The inset is the A_{454} Nernst plot from which $n = 2$ and the midpoint potential is −268 mV.

oxidation−reduction potential for PdR showed that variables associated with protein preparation and NAD(H) levels in the measurement buffer strongly influenced repeatability. Others had suggested a role for the pyridine nucleotide when using photochemical dyes or NADPH to titrate PdR preparations that were derived from P450cam proteins expressed in *P. putida* cultured with camphor (*23*, *26*). The possibility that a PdR:NAD complex could influence PdR redox potential has also been informed by earlier studies showing more than 90 mV positive shift in the reduction potential of AdR due to complex formation with $NADP^+$ (*5*). We set about building a reproducible correlation between PdR redox potential and NAD^+ influence that included a measurement on a recombinantly generated protein preparation that was repurified to ensure pyridine nucleotide-free protein. Denatured protein was washed free of pyridine nucleotide, refolded in the presence of FAD, and washed free of excess FAD. Refolded preparations gave a spectrophotometric signature that showed no free FAD absorbance and was superimposable with the characteristic peaks at 378, 454, and 480 nm of the starting material.

Figure 2 shows that addition of NAD^+ leads to the characteristic tail at long wavelengths in the PdR spectra, indicative of the formation of the PdR:NAD^+ complex (*23*). Absorbance changes in Figure 3, representing almost 4 orders of magnitude in the ratio of PdR redox species [PdR^{rd}]/[PdR^{ox}], were acquired for the Nernst plot showing a two-electron process and a midpoint potential of −369 ± 10 mV. This is significantly more negative than previously reported values of midpoint potential (*23*, *25*−*27*), but as will be described later, the data from Figure 5 indicate that it would

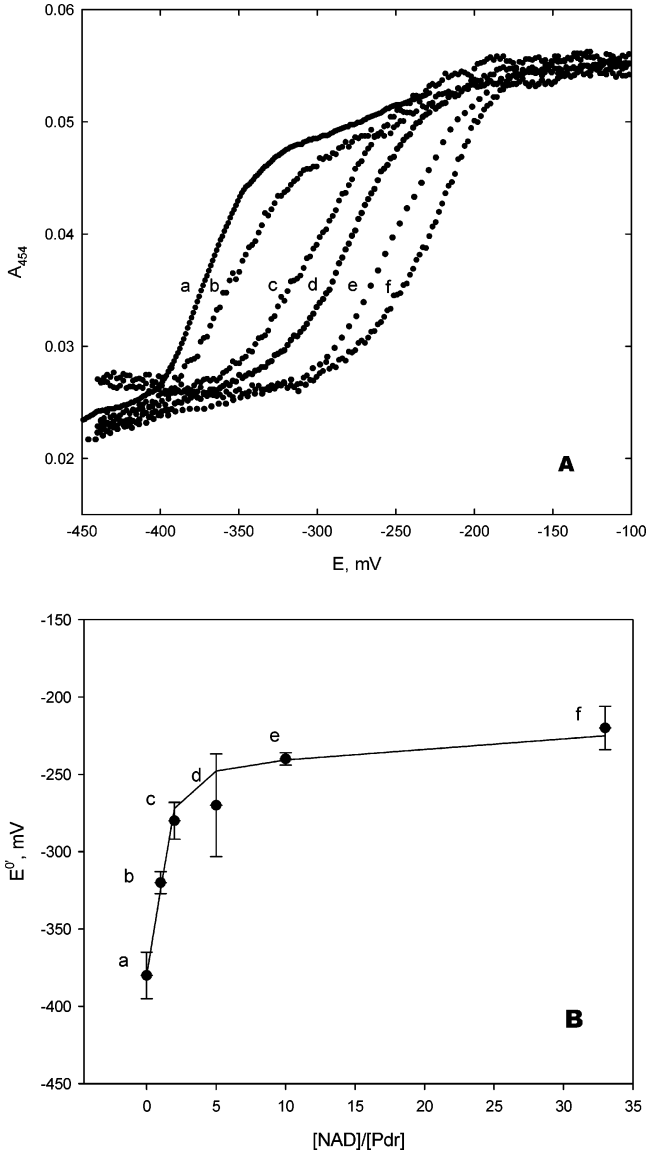

FIGURE 5: (A) Absorbance at 454 nm as a function of electrode potential for NAD-free PdR (curve a) and for PdR with added NAD^+: 9 μM NAD^+ (curve b), 18 μM NAD^+ (curve c), 45 μM NAD^+ (d), 90 μM NAD^+ (e), and 297 μM NAD^+ (f). PdR was 9 μM in solution as described in Figure 2. Panel B shows PdR redox potential as a function of the molar PdR/NAD^+ ratio, calculated from the titration curves in panel A.

only take about 1:1 NAD^+-to-PdR molar ratio (free plus bound) to shift this potential more positive by 60−80 mV, which is in the range of the previous values. The recently reported crystal structure of PdR indicates the presence of bound pyridine nucleotide that was probably copurified using commonly accepted PdR purification protocols (*1*). We also conducted PdR spectroelectrochemical titration in the presence of NADP or putidaredoxin (Pdx), the naturally occurring redox partner protein of PdR. In both cases, the midpoint reduction potential of PdR was unaffected within measurement precision. These observations are consistent with those of others who have suggested that $NADP^+$ does not form a complex with PdR (*23*) and that Pdx acts simply as an "electron shuttle" between PdR and P450cam during only a fleeting interaction with PdR (*38*).

In Figure 4, reduction of PdR in the presence of 1:5 molar ratio of NAD proceeds from right to left as the applied

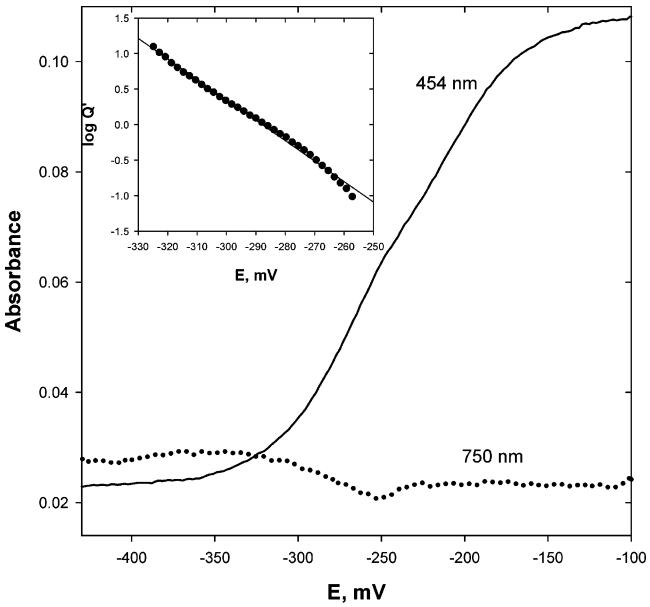

FIGURE 6: Absorbance at 454 nm (PdR reduction) and 750 nm (evolution of PdR:NAD^+ complex) as a function of electrode potential for solutions containing 9 μM PdR + 18 μM putidaredoxin + 18 μM NAD^+. The inset shows the Nernst plot for PdR reduction from which $n = 2$ and the midpoint potential is −288 mV.

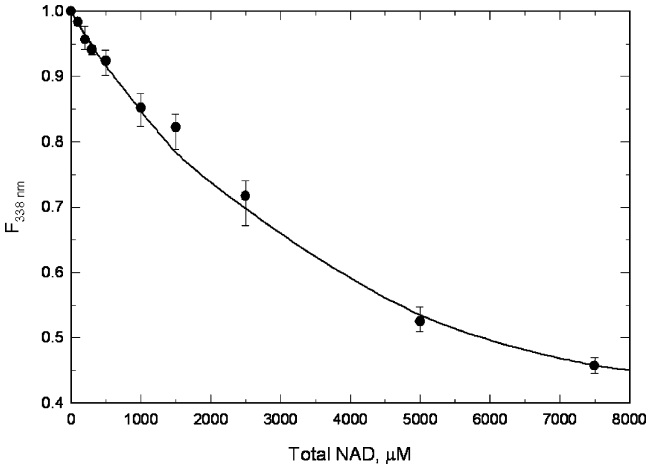

FIGURE 7: Quenching of intrinsic PdR fluorescence due to NAD^+ binding. PdR was 20 μM in 20 mM phosphate buffer + 100 mM KCl, pH 7.4 and 20 °C. The range of three determinations is shown for each NAD^+ concentration. A Scatchard fit using the equilibrium binding equation $K_D = [PdR^{ox}][NAD^+]/[PdR^{ox}{:}NAD^+]$ gives the curve shown in the figure with dissociation constant $K_D = 230 \pm 20$ μM.

potential is varied from −100 to less than −400 mV. The changes in absorbance bands at 454, 750, and 340 nm were recorded in order to establish the sequence of PdR reduction, PdR:NAD^+ charge-transfer complex formation, and free NAD^+ reduction to NADH, respectively. The transitions in the 454 and 750 nm absorbance bands as $E = -190 \rightarrow -300$ mV, and the Nernst plot showing that these transitions are accompanied by a two-electron-transfer process, suggest that the charge-transfer process is that of $PdR^{ox}{:}NAD^+ \rightarrow PdR^{rd}{:}NAD^+$ with a reduction midpoint potential of −268 ± 10 mV. There were no detectable spectral signatures in the 520−600 nm range where semiquinone formation might be expected (*37*). Similar redox transitions have been investigated for the reduction of AdR during titration with dyes or NADPH. There was no clear resolution of the redox states of the AdR and $NADP^+$ partners in the charge-transfer complex (*5*, *6*).

Because in vivo concentrations of pyridine nucleotides (*39*, *40*) are likely to be orders of magnitude greater than those of reductase enzymes, we decided to measure PdR redox potential as a function of NAD^+ concentration. Figure 5 shows measurements of reduction potential up to the ratio of $[NAD^+]/[PdR] = 33$. From the most negative value for $E^{0\prime} = -369$ mV for the repurified/refolded preparation with no NAD^+, the potential approached −230 mV asymptotically at high concentrations of NAD^+. Therefore, it is likely that in a cellular environment, the effect of NAD^+ association is to shift PdR's redox potential sufficiently positive so that it is favorably positioned thermodynamically to use the reducing power of the NADH/NAD^+ couple to drive the P450 cycle.

Adrenodoxin reductase and ferredoxin−$NADP^+$ reductase (FNR) are two of the best-characterized monoflavin reductases, and each appears to have evolved an intrinsic redox character of the FAD center to fit specific functional needs. The two-electron ($n = 2$) oxidation/reduction potential of free FAD is −162 mV at pH 6, −219 mV at pH 7, and −280 mV at pH 8 (*28*). In the case of FNR, specific residues have been implicated for their effects on the redox behavior of the FAD through influence on the protonation, orientation, and distortion of the isoalloxazine ring (*19*, *20*, *22*). These influences lead to shifts in FAD redox potential to more negative values, and in the cases of AdR and FNR, to stabilization of the semiquinone state such that two superimposed reversible one-electron-transfer processes can be split into two separately measurable single-electron transfers. The large negative reduction potential for neat PdR is in the range of values reported for neat FNR ($E^{0\prime} = -342$ mV for $n = 2$, pH 7 and $E^{0\prime} = -325$ to −442 mV for $n = 2$, pH 8−8.4) from a variety of sources (spinach chloroplasts, *Anabaena* cyanobacterium, and recombinant DNA) as determined by both dye titration and spectroelectrochemical methods (*18*−*20*, *41*). For AdR, the influence of the protein matrix leads to a smaller negative shift in the FAD redox potential to $E^{0\prime} = -295$ mV, $n = 2$, pH 7.5 (*42*). The more noteworthy difference in PdR relative to FNR or AdR is the size of the positive shift in redox potential that results from binding the pyridine nucleotide ligand. For PdR, we have measured the +139 mV shift that accompanies saturation binding of NAD^+ ($[NAD^+]/[PdR] > 33{:}1$); for FNR there is a +70 mV shift upon binding of $NADP^+$ at $[NADP^+]/[FNR] \approx 2{:}1$ (*41*); for AdR there is a +93 mV shift upon binding $NADP^+$ at $[NADP^+]/[AdR] \approx 5{:}1$ (*5*). These shifts in AdR and FNR potentials are referenced to redox potentials thought to be measured on ligand-free proteins (neat AdR or neat FNR) since X-ray diffraction structures have not reported the presence of copurified $NADP^+$ for either AdR (*22*) or FNR (*43*). If, however, the AdR and FNR redox potentials are as sensitive to small concentrations of oxidized pyridine nucleotide shown for PdR in Figure 5B, it would take as little as 2−3 μM of $NADP^+$ (free plus bound) to increase the redox shifts of AdR:$NADP^+$ or FNR:$NADP^+$ by an additional 60 mV, which is then in the range of the PdR:NAD^+ redox potential.

Binding of NAD^+ to PdR^{ox} and PdR^{rd}. Although formation of a charge-transfer complex between NAD^+ and PdR^{rd} has been known for a long time (*26*), and the spectral features

Scheme 1: Association and Redox Equilibria for Putidaredoxin Reductase−Nad^+ Complex

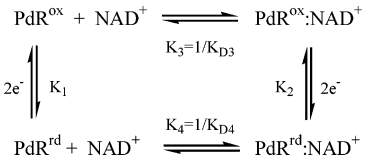

Table 1: Redox and Binding Equilibria Parameters for Putidaredoxin Reductase and Nad^+

reaction	measurements	ΔG, meV[a]	K_D, M
(1) $PdR^{ox} + 2e^- \leftrightarrow PdR^{rd}$	$E^{0\prime} = -369 \pm 10$ mV	+742	
(2) $PdR^{ox}:NAD^+ \leftrightarrow PdR^{rd}:NAD^+$	$E^{0\prime} = -230 \pm 10$ mV	+462	
(3) $PdR^{ox} + NAD^+ \leftrightarrow PdR^{ox}:NAD^+$	$K_{D3} = 230 \pm 30\ \mu$M	−212	2.30×10^{-4}
(4) $PdR^{rd} + NAD^+ \leftrightarrow PdR^{rd}:NAD^+$		−492[b]	3.58×10^{-9}

[a] Calculated from $\Delta G = 2FE^{0\prime}$ or $\Delta G = RT \ln K_D$. [b] $\Delta G_4 = \Delta G_2 + \Delta G_3 - \Delta G_1$.

at long wavelengths have been described (*23*), measurement of binding equilibria or kinetic characterization have not been possible due to the high affinity and rapid association of the ligand−protein complex. Similarities in the spectra, binding equilibria, and kinetics between the $PdR^{rd}:NAD^+$ complex and that of $AdR^{rd}:NADP^+$ (for which K_D has been calculated to be 0.01 μM (*5*)) led us to do a free energy coupling calculation of pyridine nucleotide binding to PdR^{ox} with the redox potential shift, thereby completely characterizing the redox and binding equilibrium.

$PdR^{ox}:NAD^+$ complex formation, determined from fluorescence quenching of free PdR as a function of NAD^+ concentration (Figure 7), provided a simple Scatchard binding isotherm from which K_D was determined to be 230 ± 30 μM. This is more than 16-fold larger than K_D for the charge-transfer complexes $AdR^{ox}:NADP^+$ (14 μM) (*5*), $FNR^{ox}:NADP^+$ (6−14 μM) (*32*, *44*), or the reductase component of cytochrome $P450_{BM3}$, $BMR^{ox}:NADP^+$ (10 μM) (*35*); however, it is only 7-fold higher than K_D for $PdR^{ox}:NADH$ (*26*) which is the preferred ligand in a catalytically competent process.

The redox potential measurements are used to calculate the free energies of reactions 1 and 2 in Scheme 1 and are combined with the $PdR^{ox}:NAD^+$ binding free energy to determine the dissociation constant for NAD^+ binding to reduced PdR: $\Delta G_4 = \Delta G_2 + \Delta G_3 - \Delta G_1$ and $K_{D4} = \exp(\Delta G_4/RT)$.

These data and calculations, summarized in Table 1, show that NAD^+ binding to the reduced form of PdR (K_{D4} = 0.00358 μM) is almost 5 orders of magnitude stronger than to the oxidized form. Comparable data sets for estimating $NADP^+$ binding to reduced AdR and FNR reductases are not available, although on the basis of potential shift measurements alone, binding of oxidized pyridine nucleotides to the reduced forms of these reductases is much stronger than to their oxidized forms (*5*, *17*). In a recent paper, Tejero et al. used stopped flow kinetic experiments with multi-wavelength spectroscopic measurements and a deconvolution algorithm to isolate a spectral signal for each charge-transfer species in the equilibrium reaction $FNR^{ox}:NADPH \leftrightarrow FNR^{rd}:NADP^+$ (*45*). Their estimate for the upper limit $K_{D4} < 0.2$ μM is about 50-fold lower than the range cited above for $FNR^{ox}:NADP^+$ binding, $K_{D3} \approx 6-14$ μM (*32*, *44*).

Comparative Pathways of Electron Transfer to and from Monoflavin Reductases. The function of PdR is the same as AdR and FNR. In catalyzing the reaction of pyridine nucleotide oxidation/reduction to ferredoxin reduction/oxidation, the three reductases display large asymmetries in binding equilibria that result from the intermolecular electron transfers and act as two-to-one electron transformers between the NAD(P)H and ferredoxin redox partners. The measurements reported here reveal that PdR is different only in regard to the degree of these common features: (i) lower affinity in the oxidized state for its natural oxidized pyridine nucleotide partner, (ii) greater affinity in the reduced state for the oxidized pyridine nucleotide, and (iii) greater instability of the isoalloxazine semiquinone redox state. Although the intent of this study was not to develop a mechanistic model of the in vivo redox catalysis carried out by these reductases, the compulsory ordered pathway of Figure 8 is proposed in order to show how these features work together with the large amount of kinetic and structural data that has been generated on these three systems over the last 3 decades. The pathway splits the two-electron reducing equivalents received by the reductase (Rd) from a reduced pyridine nucleotide (NH) into two separate one-electron transfers to partner ferredoxin proteins (Fx). This scheme has been considered as an electron-transfer model (in the reverse direction of Figure 8) for the Fd/FNR/NADP(H) system during photosynthesis (*13*) and as part of an earlier proposed model based on kinetic measurements in the NAD(H)/PdR/Pdx system (*24*).

Several features can be brought together from the reported X-ray diffraction structures of these reductases to support an ordered pathway. First, separate binding domains for the pyridine nucleotides and ferredoxin are observed for the FNR:Fd complex (*46*) and are to be expected from the analysis that accompanies the structure reports for AdR (*22*) and PdR (*1*). Second, close separation of the FAD and iron−sulfur redox centers upon Rd:Fx binding is observed in the FNR:Fd complex, about 6 Å (*46*), and is derived from modeling studies for the AdR:Adx complex, 11−15 Å (*22*), and for PdR:Pdx complex, ∼15 Å (*4*). Third, some stabilization of the semiquinone form in AdR and FNR is achieved by hydrogen bonds to the isoalloxazine N5 atom from active site side-chain residues in the case of FNR (*47*) or immobilized water in the case of AdR (*22*). Although such hydrogen bond stabilization is missing in PdR (*1*), a very short-lived semiquinone form has been observed by laser flash photolysis techniques (*48*). These features support the concepts of (i) ternary complexes Rd_{N+}:Fx between the two separate one-electron transfers to Fx, (ii) rapid Rd→Fx electron transfer, and (iii) difficulty of semiquinone detection in PdR relative to detection in AdR and FNR.

Considering all reported kinetic studies on these three reductases, rates for individual steps in the ordered pathway shown in Figure 8 reveal that the lifetimes of specific intermediate species are highly dependent on whether the redox components (NH, Rd, and Fx) are studied individually, in pairs, or altogether. Among many examples to illustrate this point is our observation of a decrease in the absorbance at long wavelengths, suggesting that, in the presence of Pdx, the $PdR:NAD^+$ charge-transfer complex is diminished. Also,

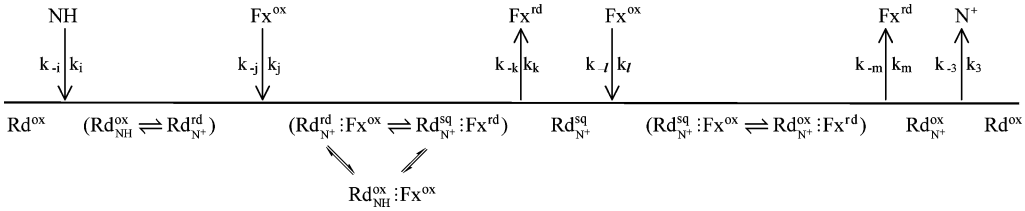

FIGURE 8: Possible compulsory ordered pathway for the transfer of two-electron reducing equivalents from a pyridine nucleotide NH (NADH or NADPH) to a monoflavin reductase Rd (putidaredoxin reductase PdR, adrenodoxin reductase AdR, or ferredoxin−NADP$^+$ reductase FNR), followed by two consecutive one-electron transfers from fully reduced reductase Rdrd, and the semiquinone reductase Rd^{sq} to a ferredoxin Fx (putidaredoxin Pdx, adrenodoxin Adx, or ferredoxin Fd). Other terms in the figure represent the following: Rd^{ox}_{NH}, or $Rd^{rd}_{N^+}$, or $Rd^{sq}_{N^+}$ are the complexes PdR:NAD$^+$, or AdR:NADP$^+$, or FNR:NADP$^+$ with the reductase in either the fully oxidized (ox), fully reduced (rd), or semiquinone (sq) oxidation state; Fx^{ox} and Fxrd are the oxidized and reduced forms of Pdx, Adx, or Fd; ternary complexes of pyridine nucleotide, reductase, and ferredoxin (e.g., PdR^{ox}:NAD$^+$:Pdxrd) are represented as $Rd^{ox}_{N^+}$:Fxrd.

K_D for the FNR:NADP$^+$ complex increases from 14 μM with no Fd present to 311 μM at 4.6 μM Fd (*34*), and ionic strength and NAD$^+$ concentration have significant effects on the rate of disproportionation of semiquinone to fully reduced and fully oxidized PdR (*48*).

The initial step in the ordered pathway is formation of the charge-transfer complex, (Rd^{ox}_{NH}, which rapidly equilibrates with its charge-transfer counterpart ($Rd^{rd}_{N^+}$). In the AdR and FNR systems, the on-rate of this step is $k_i = 28$ and $\sim$300 s^{-1}, respectively, when equimolar mixtures of NADPH and the reductase are mixed, but on-rates drop significantly when excess NADPH is present (*5*, *17*, *34*, *45*). In these studies, an equilibrium distribution of the charge-transfer species (Rd^{ox}_{NADPH} ↔ $Rd^{rd}_{NADP^+}$) was formed by either mixing oxidized pyridine nucleotide with reduced reductase or by mixing reduced pyridine nucleotide with oxidized reductase. For FNR, rates of hydride transfer between the equilibrium species were found to be at least as high as the on-rates, and for AdR and FNR the off-rates k_{-i} were found to be slow relative to on-rates. For the PdR system, the on-rate for NADH is extremely fast, $k_i > 600$ s^{-1}, and the inability to resolve the charge-transfer species (PdR^{ox}_{NADH} ↔ $PdR^{rd}_{NAD^+}$) (*23*) would be consistent with the view that the charge-transfer rate is much greater than rates of pyridine nucleotide association or dissociation.

Rates of association and electron transfer of the reduced charge-transfer complex (Rd^{ox}_{NH} ↔ $Rd^{rd}_{N^+}$) with partner ferredoxins (Fx^{ox} and Fxrd) have also been investigated for AdR (*49*−*51*), FNR (*44*, *52*, *53*), and PdR (*4*, *24*, *48*). These measurements are complicated due to rapid reoxidation of Fxrd by even traces of oxygen and by difficulties in distinguishing the two rapid one-electron transfers, $Rd^{rd/sq}_{N^+}$ → Fx and $Rd^{sq/ox}_{N^+}$ ↔ Fx. For the adrenodoxin system, stopped flow techniques show that semiquinone $AdR^{sq}_{N^+}$ is formed when equimolar NADPH and AdR^{ox} (two-electron reduction) are mixed with an equimolar amount of $Fe_3(CN)_6^{3-}$ (one-electron oxidation) and that the first electron transfer to Adx from the preformed AdR:NADP$^+$:Adx complex is faster than the second electron transfer (*49*). Formation and breakdown of the AdR:Adx complex is rapid compared to the intermolecular electron-transfer rate, and complex association is weakened upon Adx reduction (*50*, *51*). For the ferredoxin−NADP$^+$ reductase photosynthesis system operating in reverse of Figure 8, the essential features of (i) facilitation of Fd ↔ FNR electron exchange by NADP$^+$, (ii) the rapidly equilibrating ternary complex ($FNR^{sq}_{NADP^+}$:Fd^{ox} ↔ $FNR^{ox}_{NADP^+}$:Fdrd), and (iii) a sequential order of binding to FNR have been suggested (*53*). A ping−pong reaction mechanism has also been ruled out (*53*), as is to be expected when both substrates have separate binding domains. For the putidaredoxin system, steady-state and rapid stopped flow kinetic measurements using the cytochrome *c* reduction assay (Pdxrd + cyt *c*^{ox} → Pdx^{ox} + cyt *c*rd) have shown that the ternary complex is the activated redox species for describing the rates of cytochrome *c* reduction (*24*). Although the PdR^{sq} redox species was not identified, the second electron-transfer step $PdR^{sq/ox}_{NAD^+}$ → Pdx was much slower than the first, and classic ping−pong kinetics did not fit measurements of cytochrome *c* reduction when concentrations of the three redox component species, NADH/NAD$^+$, Pdx, and PdR, were varied (*24*).

Finally, we note that in vitro measurements of the reduction of the one-electron acceptors cytochrome *c* and ferricyanide have been used extensively in steady-state and rapid stopped flow experiments to test the kinetic limitations in these three systems. Under conditions of excess pyridine nucleotide and ferredoxin, steady-state cytochrome *c* reduction turns over the flavin of PdR at 550 s^{-1} (*27*), which is faster than ferredoxin−NADP$^+$ reductase flavin turnover, 200 s^{-1} (*44*), and much faster than adrenodoxin reductase flavin turnover, 4.5 s^{-1} (*5*). These higher rates for PdR activity may be consistent with its lower affinity for its oxidized pyridine nucleotide partner relative to the affinity of AdR^{ox} and FNR^{ox} for NADP$^+$, the last step in Figure 8. However, it is worth considering the relevance of the cytochrome *c* reduction assay to in vivo activity of PdR. In vivo, the function of PdR is to maintain sufficient reduced Pdx such that P450cam can maintain a viable rate of hydrocarbon conversion to meet metabolic needs. In this intracellular environment, rates of diffusive transport and intrinsic chemical conversion of hydrocarbon and oxygen cosubstrates are probably more limiting than availability of reduced Pdx, the needs for which are likely supplied by rates well below the rates of in vitro cytochrome *c* reduction. To this point, it is noteworthy that the intracellular ratio of the three proteins is estimated as 1:8:8 for PdR:Pdx:P450cam (*27*). To our knowledge, no in vitro experiments varying the multiple P450cam substrates (oxygen, hydrocarbon, putidaredoxin) required to complete the catalytic cycle have been done to investigate the rate-limiting steps of diffusion, electron transfer, or intrinsic chemical kinetics at concentrations approaching in vivo significance.

REFERENCES

1. Sevrioukova, I. F., Li, H., and Poulos, T. L. (2004) Crystal structure of putidaredoxin reductase from *Pseudomonas putida*, the final structural component of the cytochrome P450cam monooxygenase, *J. Mol. Biol. 336*, 889−902.
2. Holden, M., Mayhew, M. P., Bunk, D., Roitberg, A., and Vilker, V. L. (1997) Probing the interactions of putidaredoxin with redox partners in camphor P450 5-monooxygenase by mutagenesis of surface residues, *J. Biol. Chem. 272*, 21720−21725.
3. Sevrioukova, I. F., and Poulos, T. L. (2002) Putidaredoxin reductase, a new function for an old protein, *J. Biol. Chem. 277*, 25831−25839.
4. Kuznetsov, V. Y., Blair, E., Farmer, P. J., Poulos, T. L., Pifferitti, A., and Sevrioukova, I. F. (2005) The putidaredoxin reductase−putidaredoxin electron transfer complex: theoretical and experimental studies, *J. Biol. Chem. 280*, 16135−16142.
5. Lambeth, J. D., and Kamin, H. (1976) Adrenodoxin reductase: properties of the complexes of reduced enzyme with $NADP^+$ and NADPH, *J. Biol. Chem. 251*, 4299−4306.
6. Kitagawa, T., Sakamoto, H., Sugiyama, T., and Yamano, T. (1982) Formation of the semiquinone form in the anaerobic reduction of adrenodoxin reductase by NADPH, *J. Biol. Chem. 257*, 12075−12080.
7. Muller, J. J., Lapko, A., Bourenkov, G., Ruckpaul, K., and Heinemann, U. (2001) Adrenodoxin reductase−adrenodoxin complex structure suggests electron transfer path in steroid biosynthesis, *J. Biol. Chem. 272*, 2786−2789.
8. Sligar, S. G., and Gunsalus, I. C. (1976) A thermodynamic model of regulation: modulation of redox equilibria in camphor monooxygenase, *Proc. Natl. Acad. Sci. U.S.A. 73*, 1078−1082.
9. Sligar, S. G. (1976) Coupling of spin, substrate, and redox equilibria in cytochrome P450, *Biochemistry 15*, 5399−5406.
10. Griffin, B. W., and Peterson, J. A. (1972) Camphor binding by pseudomonas putida cytochrome P-450. Kinetics and thermodynamics of the reaction, *Biochemistry 11*, 4740−4746.
11. Hintz, M. J., Mock, D. M., Peterson, L. L., Tuttle, K., and Peterson, J. A. (1982) Equilibrium and kinetic studies of the interaction of cytochrome P-450cam and putidaredoxin, *J. Biol. Chem. 257*, 14324−14332.
12. Kuznetsov, V. Y., Poulos, T. L., and Sevrioukova, I. F. (2006) Putidaredoxin-to-cytochrome P450cam electron transfer: differences between the two reductive steps required for catalysis, *Biochemistry 45*, 11934−11944.
13. Carrillo, N., and Ceccarelli, E. A. (2003) Open questions in ferredoxin−$NADP^+$ reductase catalytic mechanism, *Eur. J. Biochem. 270*, 1900−1915.
14. Iyanagi, T., Makino, N., and Mason, H. S. (1974) Redox properties of reduced nicotinamide adenine dinucleotide phosphate−cytochrome P-450 and reduced nicotinamide adenine dinucleotide−cytochrome *b reductases*, *Biochemistry 13*, 1701−1710.
15. Vermilion, J. L., Ballou, D. P., Massey, V., and Coon, M. J. (1981) Separate roles for FMN and FAD in catalysis by liver microsomal NADPH−cytochrome P-450 reductase, *J. Biol. Chem. 256* 266−277.
16. Oprian, D. D., and Coon, M. J. (1982) Oxidation−reduction states of FMN and FAD in NADPH−cytochrome P-450 reductase during reduction by NADPH, *J. Biol. Chem. 257*, 8935−8944.
17. Batie, C. J., and Kamin, H. (1986) Association of ferredoxin−$NADP^+$ reductase with NADP(H) specificity and oxidation−reduction properties, *J. Biol. Chem. 261*, 11214−11223.
18. Corrado, M. E., Aliverti, A., Zanetti, C., and Mayhew, S. G. (1996) Analysis of the oxidation−reduction potentials of recombinant ferredoxin−$NADP^+$ reductase from spinach chloroplasts, *Eur. J. Biochem. 239*, 662−667.
19. Faro, M., Gomez-Moreno, C., Stankovich, M., and Medina, M. (2002) Role of critical charged residues in reduction potential modulation of ferredoxin−$NADP^+$ reductase: Differential stabilization of FAD redox forms, *Eur. J. Biochem. 269*, 2656−2661.
20. Hurley, K. J., Weber-Main, A. M., Stankovich, M. T., Benning, M. M., Thoden, J. B., Vanhooke, J. L., Holden, H. M., Chae, Y. K., Xia, B., Cheng, H., Markley, J. L., Martinez-Julvez, M., Gomez-Moreno, C., Schmeits, J. L., and Tollin, G. (1997) Structure−function relationships in *Anabaena ferredoxin*: correlations between X-ray crystal structures, reduction potentials, and rate constants of electron transfer to ferredoxin:$NADP^+$ reductase for site-specific ferredoxin mutants, *Biochemistry 36*, 11100−11117.
21. Anusevicius, Z., Miseviciene, L., Medina, M., Martinez-Julvez, M., Gomez-Moreno, C., and Cenas, N. (2005) FAD Semiquinone stability regulates single- and two-electron reduction of quinones by *Anabaena* PCC7119 ferredoxin:$NADP^+$ reductase and its Glu301Ala mutant, *Arch. Biochem. Biophys. 437*, 144−150.
22. Ziegler, G. A., Vonrhein, C., Hanukoglu, I., and Schulz, G. E. (1999) The structure of adrenodoxin reductase of mitochondrial P450 systems: electron transfer for steroid biosynthesis, *J. Mol. Biol. 289*, 901−990.
23. Roome, P. W., and Peterson, J. A. (1988) The reduction of putidaredoxin reductase by reduced pyridine nucleotides, *Arch. Biochem. Biophys. 266*, 32−40.
24. Roome, P. W., and Peterson, J. A. (1988) The oxidation of reduced putidaredoxin reductase by oxidized putidaredoxin, *Arch. Biochem. Biophys. 266*, 41−50.
25. Gunsalus, I. C., Meeks, J. R., Lipscomb, J. D., Debrunner, P., and Munck, E. (1974) Bacterial Monooxygenase−The P450 Cytochrome System, in *Molecular Mechanisms of Oxygen Activation* (Hayashi, O., Ed.) pp 559−613, Academic Press, New York.
26. Gunsalus, I. C., and Sligar, S. G. (1978) Oxygen reduction by the P-450 monoxygenase systems, *Adv. Enzymol. 47*, 1−44.
27. Roome, P. W., Philley, J. C., and Peterson, J. A. (1983) Purification and properties of putidaredoxin reductase, *J. Biol. Chem. 258*, 2593−2598.
28. Alberty, R. A. (2006) Oxidoreductase Reactions, *Biochemical Thermodynamics: Applications of Mathematica*, Chapter 8, John Wiley & Sons, Inc., Hoboken, NJ.
29. Backes, W. L. (1993) NADPH−Cytochrome P450 Reductase: Function, in *Handbook of Experimental Pharmacology Vol. 105: Cytochrome P450* (Schenkman, J. B., and Greim, H., Eds.) pp 15−34, Springer-Verlag, Berlin and New York.
30. Hefti, M. H., Vervoort, J., and van Berkel, W. J. H. (2003) Deflavination and reconstitution of flavoproteins: tackling fold and function, *Eur. J. Biochem. 270*, 4227−4242.
31. Reipa, V., Mayhew, M. P., and Vilker, V. L. (1997) A direct electrode-driven P450 cycle for biocatalysis, *Proc. Natl. Acad. Sci. U.S.A. 94*, 13554−13558.
32. Reipa, V., Mayhew, M. P., Holden M. J., and Vilker V. L. (2002) Redox control of the P450cam catalytic cycle: effects of Y96F active site mutation and binding of a non-natural substrate, *Chem. Commun.*, 318−319.
33. Reipa, V., Shanklin, J., and Vilker V. L. (2004) Substrate binding and the presence of ferredoxin affect the redox properties of soluble plant Δ^9-18:0-acyl carrier protein desaturase, *Chem. Commun.*, 2406−2407.
34. Batie, C. J., and Kamin, H. (1984) Ferredoxin−$NADP^+$ oxidoreductase: Equilibria in binary and ternary complexes with $NADP^+$ and ferredoxin, *J. Biol. Chem. 259*, 8832−8839.
35. Murataliev, M. B., and Feyereisen, R. (2000) Functional interactions in cytochrome P450BM3. Evidence that NADP(H) binding controls redox potentials of the flavin cofactors, *Biochemistry 39*, 12699−12707.
36. Beattie, B. K., and Merrill, A. R. (1999) A fluorescence investigation of the active site of *Pseudomonas aeruginosa* exotoxin A, *J. Biol. Chem. 274*, 15646−15654.
37. Massey, V., and Ghisla, S. (1974) Role of charge-transfer interactions in flavoprotein catalysis, *Ann. N.Y. Acad. Sci. 227*, 446−465.
38. Purdy, M. M., Koo, L. S., Ortiz de Montellano, P. R., and Klinman, J. P. (2004) Steady-state kinetic investigation of cytochrome P450cam: interaction with redox partners and reaction with molecular oxygen, *Biochemistry 43*, 271−281.
39. Leonardo, M. R., Dailly, Y., and Clark, D. P. (1996) Role of NAD in regulating the *adhE* gene of *Escherichia coli*, *J. Bacteriol. 178*, 6013−6018.
40. De Graef, M. R., Alexeeva, S., Snoep, J. L., and de Mattos, M. J. T. (1999) The steady-state internal redox state (NADH/NAD) reflects the external redox state and is correlated with catabolic adaptation in *Escherichia coli*, *J. Bacteriol. 181*, 2351−2357.
41. Batie, C. J., and Kamin, H. (1981) The relation of pH and oxidation−reduction potential to the association state of the ferredoxin::ferredoxin:$NADP^+$ reductase complex, *J. Biol. Chem. 256*, 7756−7763.
42. Lambeth, J. D., McCaslin, D. R., and Kamin, H. (1976) Adrenodoxin reductase:adrenodoxin complex−catalytic and thermodynamic properties, *J. Biol. Chem. 251*, 7545−7550.
43. Deng, Z., Aliverti, A., Zanetti, G., Arakaki, A. K., Ottado, J., Orellano, E. G., Calcaterra, N. B., Ceccarelli, E. A., Carrillo, N.,

and Karplus, P. A. (1999) A productive $NADP^+$ binding mode of ferredoxin−$NADP^+$ reductase revealed by protein engineering and crystallographic studies, *Nat. Struct. Biol. 6*, 847−853.

44. Medina, M., Martinez-Julvez, M., Hurley, J. K., Tollin, G., and Gomez-Moreno, C. (1998) Involvement of glutamic acid 301 in the catalytic mechanism of ferredoxin−$NADP^+$ reductase from *Anabaena* PCC 7119, *Biochemistry 37*, 2715−2728.
45. Tejero, J., Peregrina, J. R., Martinez-Julvez, M., Gutierrez, A., Gomez-Moreno, C., Scrutton, N. S., and Medina, M. (2007) Catalytic mechanism of hydride transfer between $NADP^+$/H and ferredoxin−$NADP^+$ reductase from *Anabaena* PCC 7119, *Arch. Biochem. Biophys. 459*, 79−90.
46. Kurisu, G., Kusunoki, M., Katoh, E., Yamazaki, T., Teshima, K., Onda, Y., Kimata-Ariga, Y., and Hase, T. (2001) Structure of the electron transfer complex between ferredoxin and ferredoxin−$NADP^+$ reductase, *Nat. Struct. Biol. 8*, 117−121.
47. Bruns, C. M., and Karplus, P. A. (1995) Refined crystal structure of spinach ferredoxin reductase at 1.7 Å resolution: oxidized, reduced and 2′-phospho-5′-AMP bound states, *J. Mol. Biol. 247*, 125−145.
48. Sevrioukova, I. F., Hazzard, J. T., Tollin, G., and Poulos, T. L. (2001) Laser flash induced electron transfer in P450cam monooxygenase: putidaredoxin reductase−putidaredoxin interaction, *Biochemistry 40*, 10592−10600.
49. Lambeth, J. D., and Kamin, H. (1977) Adrenodoxin reductase and adrenodoxin: mechanisms of reduction of ferricyanide and cytochrome *c*, *J. Biol. Chem. 252*, 2908−2917.
50. Lambeth, J. D., Seybert, D. W., and Kamin, H. (1980) Adrenodoxin reductase adrenodoxin complex: rapid formation and breakdown of the complex and a slow conformational change in the flavoproteins, *J. Biol. Chem. 255*, 4667−4672.
51. Grinberg, A. V., Hannemann, F., Schiffler, B., Muller, J., Heinemann, U., and Bernhardt, R. (2000) Adrenodoxin: structure, stability, and electron transfer properties, *Proteins: Struct., Funct., Genet. 40*, 590−612.
52. Martinez-Julvez, M., Hermoso, J., Hurley, J. K., Mayoral, T., Sanz-Aparicio, J., Tollin, G., Gomez-Moreno, C., and Medina, M. (1998) Role of Arg100 and Arg264 from *Anabaena* PCC 7119 ferredoxin−$NADP^+$ reductase for optimal $NADP^+$ binding and electron transfer, *Biochemistry 37*, 17680−17691.
53. Batie, C. J., and Kamin, H. (1984) Electron transfer by ferredoxin: $NADP^+$ reductase rapid-reaction evidence for participation of a ternary complex, *J. Biol. Chem. 259*, 11976−11985.

BI7012118